BNL-230130-2026-TECH

Analytical Dynamic Aperture Calculation Compared to Tracking Results

H. Lovelace III

August 2026

Electron-Ion Collider

Brookhaven National Laboratory

U.S. Department of Energy

USDOE Office of Science (SC), Nuclear Physics (NP)

DISCLAIMER

Analytical Dynamic Aperture Calculation Compared to Tracking Results

H. Lovelace III

August 21, 2026

Abstract
In studying dynamic aperture in the storage rings, it is becoming increasing beneficial to understand the growth of the fractal boundary of the dynamic aperture without tracking for millions of turns in an hadron ring. This note describes the J. Gao theory applied to the Electron Ion Collider (EIC) Hadron Storage Ring (HSR) and compares simulation results to theoretical predictions to show that the analytical method may prove useful in quick determinations of improved dynamic aperture based on sextupole and octupole configurations.

1 Introduction

Dynamic aperture studies for hadron closed geometry accelerators are computationally expensive due to the need of single particle tracking over many turns ($\sim 1 \times 10^7$ turns) [1]. This requires that the program runs for extended periods on the order of hours, days, or even weeks depending on the processing power. There must be a line drawn to the extent in which the accelerator community requests stronger, more powerful computers and start to investigate more clever mathematics. Analytical methods in solving for dynamic aperture (DA) have been investigated on numerous occasions [2, 3, 4], with more focus on the actual size of the DA and not the value in understanding if these methods can be use to increase the DA. In this technical note, we will explore the use of an analytical model in not only determining the DA but also increasing the DA with comparison to tracking results.

1.1 Theory

We first start with the simple Hamiltonian that describes the system with of a charged particle moving through a electromagnetic field with a given position, $\mathbf{q}$, and momentum, $\mathbf{p}$ at a given time, t. The magnetic vector potential $\mathbf{A}$, and electric scalar potential Φ [5],

$$\mathcal{H}(\mathbf{q}, \mathbf{p}, t) = e\mathbf{\Phi} + c\sqrt{(\mathbf{p} - e\mathbf{A})^2 + m_0^2 c^2}, \tag{1}$$

where c is the speed of light, m_0 is the rest mass of the particle and e is the charge of an electron. The vector potential, A_s, is expanded into a complex series,

$$A_s = \sum_n A_n (x + iy)^n. \tag{2}$$

The series $(x+iy)^n$ within A_s have real and imaginary terms that correspond to the normal and the skew components of the multipoles, respectively. The canonical pair of coordinates used are $\mathbf{q}$ and $\mathbf{p}$ where q_i and p_i are the position and momentum components of the conjugate pairs.

The equation of motion are

$$\begin{aligned}\frac{dp_i}{dt} &= -\frac{\partial \mathcal{H}}{\partial q_i} \\ \frac{dq_i}{dt} &= \frac{\partial \mathcal{H}}{\partial p_i}.\end{aligned} \tag{3}$$

From a coordinate transformation to Frenet-Serret curvilinear coordinate system, where $t \rightarrow s$ which simplifies the analysis of the trajectory of the particle, we have

$$\mathbf{H}_s = -eA_s - (1-\kappa x)\sqrt{\frac{H^2 - m_0^2c^4}{c^2} - (p_x - eA_x)^2 + (p_y - eA_y)^2}, \tag{4}$$

where κ is the inverse of the bending radius of the dipole, ρ^{-1}. Following J. Gao's [4] treatment of the Hamiltonian, we have

$$\begin{aligned}H = \frac{B_y|_{x=0,y=0}x^2}{2\rho^2 B_0} + \frac{1}{B_0\rho}\sum_{n=1}^{\infty}\frac{1}{n!}\frac{\partial^{n-1}B_y}{\partial x^{n-1}}|_{x=0,y=0}(x+iy)^n \\ -(1-\kappa x)\sqrt{\frac{P}{P_0} - (\bar{p_x} - \frac{eA_x}{P_0})^2 - (\bar{p_y} - \frac{eA_y}{P_0})^2},\end{aligned} \tag{5}$$

where the magnetic field, $\mathbf{B}$, is expanded to the n$^{\text{th}}$ pole using the curl of the magnetic vector potential,

$$\mathbf{B} = \nabla \times \mathbf{A}\frac{eA_s}{P_0} = -\frac{B_y x^2}{2\rho^2 B_0} - \frac{1}{B_0\rho}\sum_{n=1}^{\infty}\frac{1}{n!}\frac{\partial^{n-1}B_y}{\partial x^{n-1}}|_{x=0,y=0}(x+iy)^n \tag{6}$$

1.2 Simple Case

For the simple case of horizontal linear motion, and only transverse magnetic field, the Hamiltonian can be written as

$$H = \frac{p^2}{2} + \frac{K(s)}{2}x^2 \tag{7}$$

where the Φ is constant and the transverse magnetic vector potential components $\mathrm{A_x}$ and $\mathrm{A_y}$ equal zero. Here, $p = dx/ds$ and $K(s)$ is a periodic function where

$$K(s) = K(s+L) \tag{8}$$

and L is the ring circumference. The solution to the unperturbed Hamiltonian with an initial phase of ϕ_0 is

$$x = \sqrt{\epsilon_x \beta_x(s)}\cos(\phi(s) + \phi_0). \tag{9}$$

The phase advance, ϕ, is found through

$$\phi(s) = \int_0^s \frac{ds}{\beta_x(s)}. \tag{10}$$

To step into the nonlinear domain, a coordinate transformation is to action-angle where we can clearly distinguish the unperturbed and perturbed Hamiltonian. The coordinate transformation into the action can be written as,

$$J = \frac{\epsilon_x}{2} = \frac{1}{2\beta_x(s)}\left(x^2 + (\beta_x(s)x' - \frac{\beta_x' x}{2})^2\right) \tag{11}$$

and the phase angle is

$$\Psi = \int_0^s \frac{ds'}{\beta_x(s')} + \phi_0. \tag{12}$$

The Hamiltonian is

$$H(J,\Psi) = \frac{J}{\beta_x(s)} \tag{13}$$

To make the Hamiltonian independent of s, an additional canonical transformation must be made

$$\begin{aligned} J_0 &= J \\ \Psi_0 &= \Psi + \frac{2\pi}{L} - \int_0^s \frac{ds'}{\beta_x(s')} \\ H_0 &= \frac{2\pi\nu}{L} J_0. \end{aligned} \tag{14}$$

Recall,

$$x = \sqrt{2J_0\beta_x(s)}\cos\left(\Psi_0 - \frac{2\pi\nu}{L} + \int_0^s \frac{ds'}{\beta_x(s')}\right). \tag{15}$$

The perturbed Hamiltonian is written as

$$\begin{aligned} H &= H_0 + H_1 + H_2 \\ &= \frac{p^2}{2} + \frac{K(s)}{2}x^2 + \frac{1}{3!B\rho}\frac{\partial^2 B_z}{\partial x^2}x^3 L \sum_{k=-\infty}^{\infty}\delta(s-kL) + \frac{1}{4!B\rho}\frac{\partial^3 B_z}{\partial x^3}x^4 L \sum_{k=-\infty}^{\infty}\delta(s-kL). \end{aligned} \tag{16}$$

The H_1 and H_2 are the first and second order nonlinearities. If the longitudinal field is described by

$$B_z = B_0(1 + xb_0 + x^2 b_2 + x^3 b_3), \tag{17}$$

where B_0 is the main dipole field and b_1, b_2, and b_3 are the quadrupolar, sextupolar, and octupolar multipole fields, then the perturbed Hamiltonian transformed to action-angle is

$$H = \frac{2\pi\nu}{L}J_0 + \frac{(2J_0\beta_x(s_1))^{3/2}}{3\rho}b_2 L\cos^3\Psi_0 \sum_{k=-\infty}^{\infty}\delta(s-kL) + \frac{(J_0\beta_x(s_2))^2}{\rho}b_3 L\cos^4\Psi_0 \sum_{k=-\infty}^{\infty}\delta(s-kL) \tag{18}$$

where s_1 and s_2 are the locations of the sextupoles and octupoles within the lattice. We evaluate the Hamiltonian equations of motion as

$$\begin{aligned}
\frac{dJ_0}{ds} =& -\frac{\partial H}{\partial \Psi_0} \\
=& \frac{(2J_0\beta_x(s_1))^{3/2}}{3\rho} b_2 L \frac{d\cos^3\Psi_0}{d\Psi_0} \sum_{k=-\infty}^{\infty} \delta(s-kL) \\
& - \frac{(2J_0\beta_x(s_2))^2}{\rho} b_3 L \frac{d\cos^4\Psi_0}{d\Psi_0} \sum_{k=-\infty}^{\infty} \delta(s-kL) \\
\frac{d\Psi_0}{ds} =& \frac{\partial H}{\partial J_0} \\
=& \frac{2\pi\nu}{L} + \frac{(\sqrt{2J_0}\beta_x(s_1))^{3/2}}{\rho} b_2 L \cos^3\Psi_0 \sum_{k=-\infty}^{\infty} \delta(s-kL) \\
& + \frac{(2J_0\beta_x^2(s_2))}{\rho} b_3 L \cos^4\Psi_0 \sum_{k=-\infty}^{\infty} \delta(s-kL)
\end{aligned} \tag{19}$$

The perturbations have a periodicity of the cell length, L_{cell}, and as long as the Courant–Friedrichs–Lewy (CFL) condition,

$$\Delta t \leq L_{cell}/c \tag{20}$$

where c is the speed of light, and Δt is the adiabatic invariance breakdown interval, the differential equations eqns. 19 can be written as difference equations can be written as

$$\begin{aligned}
\bar{J_0} &= \bar{J_0}(\Psi_0, J_0) \\
\bar{\Psi_0} &= \bar{\Psi_0}(\Psi_0, J_0)
\end{aligned} \tag{21}$$

where the bar indicates the value after the previous value. Substituting these relations back into 19

$$\begin{aligned}
\bar{J_0} &= J_0 - \frac{(2J_0\beta_x(s_1))^{3/2}}{3\rho} b_2 L \frac{d\cos^3\Psi_0}{d\Psi_0} - \frac{(J_0\beta_x(s_2))^2}{\rho} b_3 L \frac{d\cos^4\Psi_0}{d\Psi_0} \\
\bar{\Psi_0} &= \Psi_0 + 2\pi\nu + \frac{\sqrt{2\bar{J_0}}\beta_x(s_1)^{3/2}}{\rho} b_2 L \cos^3\Psi_0 + \frac{2\beta_x(s_2)^2}{\rho} \bar{J_0} b_3 L \cos^4\Psi_0
\end{aligned} \tag{22}$$

From the trigonometric relation,

$$\cos^m \cos n\theta = 2^{-m} \sum_{r=0}^{m} \binom{m}{r} \cos n - 2r)\theta \tag{23}$$

we can rewrite the cubic and quartic trigonometric terms as

$$\begin{aligned}
\cos^3 &= \frac{2}{2^3}(\cos 3\theta + 3\cos\theta) \\
\cos^4 &= \frac{1}{2^4}\left(2\cos 4\theta + 8\cos 2\theta + \frac{4!}{((4/2)!)^2}\right).
\end{aligned} \tag{24}$$

The fractional tune, $\nu = m/n$ where n and m are integers, must be away from any strong resonance for the invariant tori to remain preserved under small perturbation of the motion [6]. The strength of the resonance is defined by n, the lower the order the stronger the resonance. We, this case, only investigate uncoupled systems.

From the stochasticity constraints given by Chirikov and others [7, 8, 9, 10], we have the stochasticity parameter

$$K_c = 0.971635 \tag{25}$$

where above this value diffusion begins and the motion of the particle becomes chaotic. We can write the single sextupole system as

$$\begin{aligned} \bar{J}_0 &= J_0 + \frac{(2J_0\beta_x(s_1))^{3/2}}{4\rho} b_2 L \sin 3\Psi_0 \\ \bar{\Psi}_0 &= \frac{\sqrt{2}\beta_x(s_1)^{3/2}}{\sqrt{\bar{J}_0}\rho} b_2 L \bar{J}_0 \end{aligned} \tag{26}$$

To easily show the effect of the **standard mapping** stochastic parameter, K_c, we rewrite equation 26 as

$$\begin{aligned} \bar{\zeta} &= \zeta + K_c \sin\theta \\ \bar{\theta} &= \theta + \bar{\zeta} \end{aligned} \tag{27}$$

where

$$\begin{aligned} \theta &= 3\Psi \\ \zeta &= 3J_0 \frac{(2J_0\beta_x(s_1))^{3/2}}{4\rho} b_2 L \\ K_c &= 3J_0\beta_x(s_1)^3 \big(\frac{|b_2|L}{\rho}\big)^2. \end{aligned} \tag{28}$$

Next we find the maximum J_0 for the 3[rd] order resonance,

$$J_0 \leq J_{max,sex} = \frac{1}{3\beta_x(s_1)^3}\big(\frac{\rho}{|b_2|L}\big)^2 \tag{29}$$

The dynamic aperture of the accelerator in the horizontal plane is

$$A_{dyna,sext} = \sqrt{2J_{max,sext}\beta_x(s)} = \frac{\sqrt{2\beta_x(s)}}{\sqrt{3}\beta_x(s_1)^{3/2}} \frac{\rho}{|b_2|L} \tag{30}$$

for sextupole strength. And for a single octupole, the DA is

$$A_{dyna,oct} = \sqrt{2J_{max,oct}\beta_x(s)} = \frac{\sqrt{\beta_x(s)}}{\beta_x(s_2)} \sqrt{\frac{\rho}{|b_3|L}}. \tag{31}$$

If we treat the components as independent resonators, we can have the cumulative DA,

$$A_{DA,tot} = 1/\sqrt{\sum_i \frac{1}{A^2_{DA,sex,i}} + \sum_j \frac{1}{A^2_{DA,oct,j}}}. \tag{32}$$

For the vertical plane, the crossing terms exchange energy between the two planes and

$$\beta_x(s_1)A^2_{DA,sex,x} = \beta_x(s_1)A^2_{DA,sex,y} + \beta_x(s_1)x^2 \tag{33}$$

which can be rewritten as

$$A_{DA,sex,y} = \sqrt{\frac{\beta_x(s_1)}{\beta_y(s_1}(A^2_{DA,sex,x} - x^2)} \tag{34}$$

Due to the exclusion of the phase cancellation, the method will not determine the exact dynamic aperture unless each sextupole or octupole is an independent variable in the lattice. However, the increase or decrease of the dynamic aperture be guided from only the calculation of the DA from eqns. 32.

2 Chromaticity Minimization

The baseline lattice used for the study is the `pp-100GeV-rhic-ir2` [11] lattice that have the optics shown in Fig. 1. The β^* at IP6 of the closed geometry lattice is 60 cm horizontal and 7.7 cm vertical. The working point of the lattice is 27.228 and 25.210 horizontal and vertical respectively, with natural chromaticities of -64.96 and -61.49. At store the optimal chromaticity is 2 units in both planes which is obtained through 24 sextupole families. The arcs contain 144 sextupoles separated by the 6 arcs. Each arc has 4 sextupole families per arc. For the modeling, all arc sextupoles are used with 24 families that are varied.

To allow a fair comparison, the baseline lattice linear and non-linear chromaticities were minimized using weighted multi-objective optimization written for the PyTao [12] program `bettasex.py`, which acts directly onto the chromaticity via

$$\begin{aligned}
f_1 &= \left(\frac{\chi_x^{(1)} - \text{TARGET}}{2}\right)^2 + \left(\frac{\chi_y^{(1)} - \text{TARGET}}{2}\right)^2, \\
f_2 &= \left(\frac{\chi_x^{(2)}}{10^3}\right)^2 + \left(\frac{\chi_y^{(2)}}{10^3}\right)^2, \\
f_3 &= \left(\frac{\chi_x^{(3)}}{10^6}\right)^2 + \left(\frac{\chi_y^{(3)}}{10^6}\right)^2, \\
f &= f_1 + f_2 + f_3.
\end{aligned} \tag{35}$$

where the parenthesized superscript indicates the order of chromaticity, $\chi_{x,y}$. The TARGET linear chromaticity is 2. The tune shifts from the action of the particle are

$$\begin{aligned}
\Delta\nu_x &= \frac{1}{2\pi}\frac{\partial}{\partial J_x}\left\{\frac{1}{4\ B\rho}\sum_{i=1}^{N}\left[(b_1L)_i - 2(b_2L)_i\eta^{(1)}_{xi}\right]\beta_{xi}\right\} \\
\Delta\nu_y &= -\frac{1}{2\pi}\frac{\partial}{\partial J_y}\left\{\frac{1}{4B\rho}\sum_{i=1}^{N}\left[(b_1L)_i - 2(b_2L)_i\eta^{(1)}_{xi}\right]\beta_{xi}\right\}.
\end{aligned} \tag{36}$$

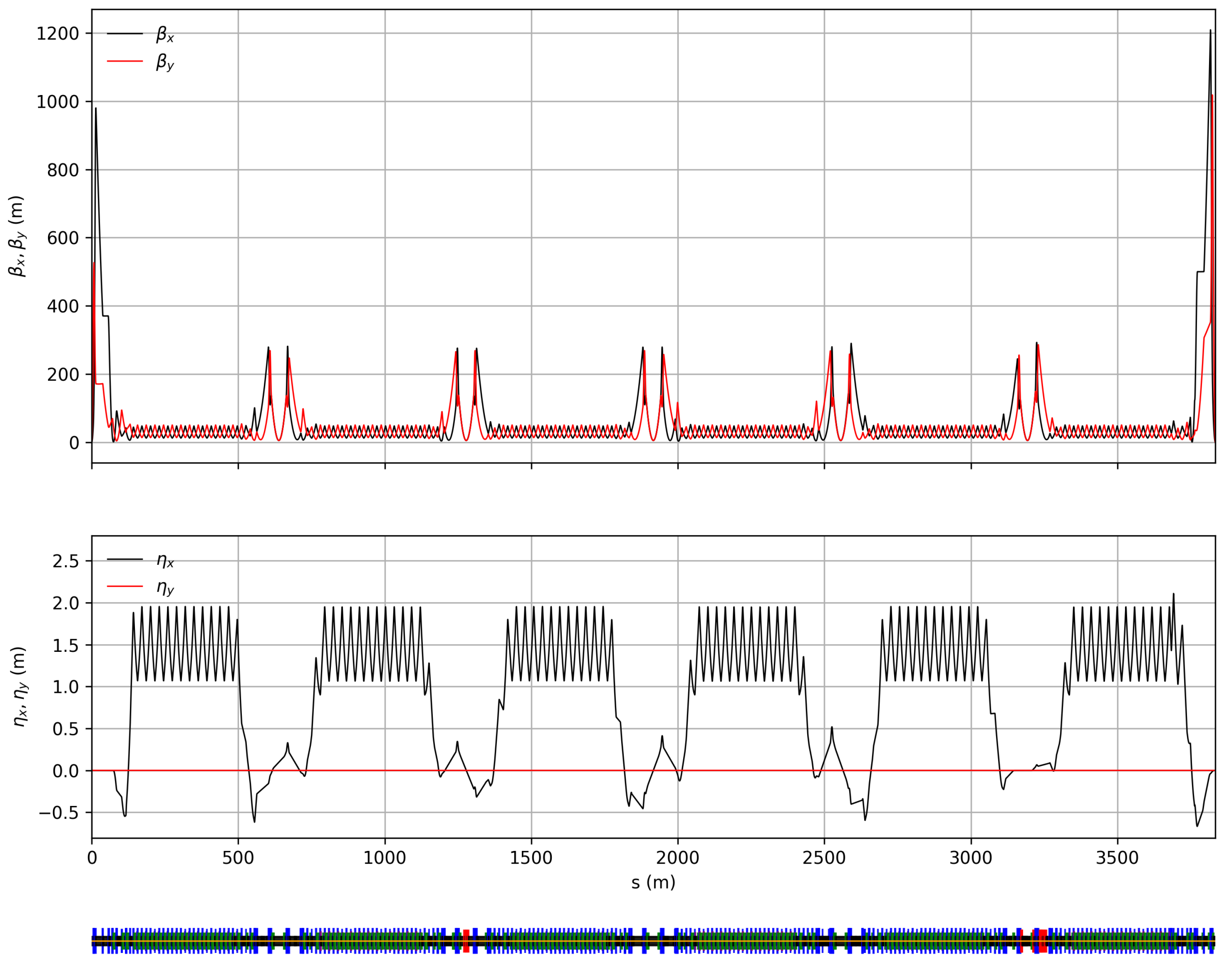

Figure 1: `pp-100GeV-rhic-ir` lattice optics. Top: Twiss Parameters, Middle: Dispersion, Bottom: Layout

The chromaticities can explicitly be written as [13, 14]

$$\chi_x^{(1)} = \left.\frac{\partial \Delta\nu_x}{\partial \delta}\right|_{\delta=0} = -\frac{1}{4\pi B\rho}\sum_{i=1}^{N}\left[(b_1L)_i - 2(b_2L)_i\eta_{xi}^{(1)}\right]\beta_{xi} \tag{37}$$

$$\chi_y^{(1)} = \left.\frac{\partial \Delta\nu_y}{\partial \delta}\right|_{\delta=0} = \frac{1}{4\pi B\rho}\sum_{i=1}^{N}\left[(b_1L)_i - 2(b_2L)_i\eta_{xi}^{(1)}\right]\beta_{yi} \tag{38}$$

$$\begin{aligned}\chi_x^{(2)} &= \frac{1}{2!}\left.\frac{\partial^2 \Delta\nu_x}{\partial \delta^2}\right|_{\delta=0} \\ &= -\frac{1}{2}\chi_x^{(1)} + \frac{1}{8\pi B\rho}\sum_{i=1}^{N}\Bigg\{2(b_2L)_i\eta_{xi}^{(2)}\beta_{xi} \\ &\qquad - \left[(b_1L)_i - 2(b_2L)_i\eta_{xi}^{(1)}\right]\beta_{xi}^{(1)}\Bigg\}\end{aligned} \tag{39}$$

$$\chi_y^{(2)} = \frac{1}{2!}\left.\frac{\partial^2 \Delta\nu_y}{\partial \delta^2}\right|_{\delta=0}$$

$$
\begin{aligned}
&= -\frac{1}{2}\chi_y^{(1)} + \frac{1}{8\pi B\rho}\sum_{i=1}^{N}\Bigg\{2(b_2L)_i\eta_{xi}^{(2)}\beta_{yi} \\
&\quad - \left[(b_1L)_i - 2(b_2L)_i\eta_{xi}^{(1)}\right]\beta_{yi}^{(1)}\Bigg\} \qquad (40)
\end{aligned}
$$

$$
\begin{aligned}
\chi_x^{(3)} &= \frac{1}{3!}\frac{\partial^3\Delta\nu_x}{\partial\delta^3}\bigg|_{\delta=0} \\
&= -\frac{1}{24\pi B\rho}\sum_{i=1}^{N}\Bigg\{\Big[2(b_1L)_i - 4(b_2L)_i\eta_{xi}^{(1)} \\
&\quad + 4(b_2L)_i\eta_{xi}^{(2)} - 2(b_2L)_i\eta_{xi}^{(3)}\Big]\beta_{xi} \\
&\quad - 2\left[(b_1L)_i\eta_{xi}^{(1)} + 2(b_2L)_i\eta_{xi}^{(2)}\right]\beta_{xi}^{(1)} \\
&\quad + \left[(b_1L)_i - 2(b_2L)_i\eta_{xi}^{(1)}\right]\beta_{xi}^{(2)}\Bigg\} \qquad (41)
\end{aligned}
$$

$$
\begin{aligned}
\chi_y^{(3)} &= \frac{1}{3!}\frac{\partial^3\Delta\nu_y}{\partial\delta^3}\bigg|_{\delta=0} \\
&= -\frac{1}{24\pi B\rho}\sum_{i=1}^{N}\Bigg\{\Big[2(b_1L)_i - 4(b_2L)_i\eta_{xi}^{(1)} \\
&\quad + 4(b_2L)_i\eta_{xi}^{(2)} - 2(b_2L)_i\eta_{xi}^{(3)}\Big]\beta_{yi} \\
&\quad - 2\left[(b_1L)_i\eta_{xi}^{(1)} + 2(b_2L)_i\eta_{xi}^{(2)}\right]\beta_{yi}^{(1)} \\
&\quad + \left[(b_1L)_i - 2(b_2L)_i\eta_{xi}^{(1)}\right]\beta_{yi}^{(2)}\Bigg\} \qquad (42)
\end{aligned}
$$

The program uses the Bmad libraries [15] to calculate the chromaticities and utilizing the Python internal optimization tools minimizes the chromaticities up to the 3$^{\text{rd}}$ order. The code can be extended to any order. The target chromaticity, as mentioned previously, is 2 units in both planes. Table 1 contains the chromaticity values for the baseline lattice. From the table, the decrease in the 2$^{\text{nd}}$ in both planes and the decrease in the absolute value of the horizontal 3$^{\text{rd}}$ chromaticity attribute to the results from tracking shown later in this note.

Table 1: Baseline and Post-Optimization (ANDA) 100 GeV lattice chromaticities using eqn. 35 and eqn. 37

	Horizontal		Vertical	
Order	Baseline	Post-Optimization	Baseline	Post-Optimization
1	2.00	2.02	2.00	1.94
2	-4.13	-232.64	-7.62	-417.08
3	-40124.98	5895.93	-60319.26	128583.56

3 Analytical Dynamic Aperture Optimizer

Using eqn. 32 the Analytical Dynamic Aperture (ANDA) program maximizes the analytically calculated DA by adjusting the sextupole strengths such that the calculated DA increasingly improves from it's initial value. This iterative process treats all sextupoles as independent resonance drivers, ignoring all phase cancellations. This approach allows the direct calculation of the Hamiltonian at each sextupole. Using this method, one can estimate the before tracking if the DA increases with a given sextupole or octupole configuration. The linear chromaticity is constrained to the target value while higher order chromaticities are left to change freely. The objective of the ANDA program is to maintain a given linear chromaticity while increasing the DA analytically.

The cumulative DA show over the chromatic sextupoles of the Electron Ion Collider (EIC) Hadron Storage Ring HSR, shows a substantial improvement when compared to the baseline lattice which is plotted in Fig. 2. The plot is of the leading sextupole term of eqn. 32. It is clear that with each sextupole, the $A^{-2}_{DA,sex}$ decreases from baseline showing an improvement to the dynamic aperture.

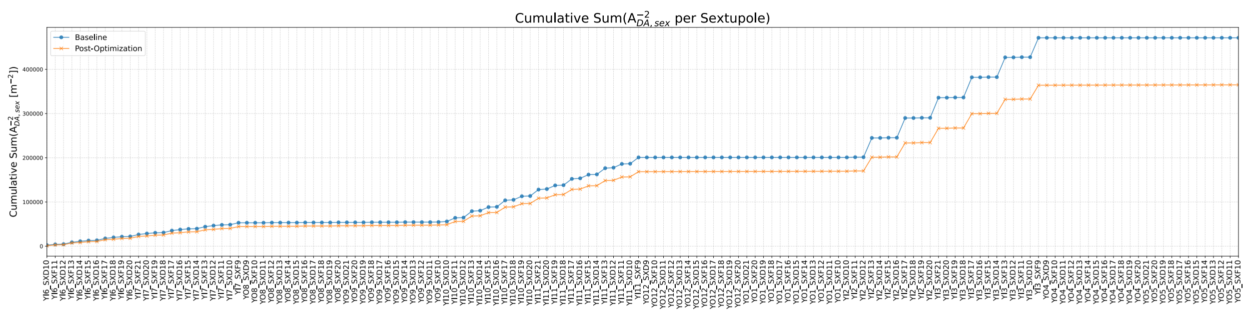

Figure 2: Cumulative increase in the A^{-2} over the sextupoles of the lattice. The x-axis shows the increase per arc sextupole of the HSR. Table in the Appendix A shows the A^{-2} for each sextupole explicitly.

4 Results

Figure 3 is a comparison of the DA over 1×10^7 turns using the Bmad [15] accelerator toolkit. The physical tracking is 4D+1, meaning the 4 transverse dimensions plus the momentum offset at a given dp/p from 0 to 0.3%. The momenta range chosen is essentially the height of the RF bucket of the HSR. The initial phase angles are from 0 to $\pi/2$ with 5 phase angles equally spaced used for initial launch conditions. The viewpoint for the DA is IP6 with the previously mentioned 60 cm horizontal and 7.7 cm vertical.

The ANDA calculates the DA horizontal and vertical pre-optimization DA to be 1.457 mm and 0.727 mm, respectively. The predicted purely horizontal DA prior to the optimization is $10.85\sigma_x$ where as the tracked value for the $10.91\sigma_x$ for the on-momentum particle. The vertical DA is $50.36\sigma_y$ with a tracked measurement of $37.1\sigma_y$ which much less than the predicted value. The vertical DA post-optimization is $60.89\sigma_y$ with a tracked value of $41.10\sigma_y$. In the vertical plane, the DA predictions starts to breakdown. From tracking alone, the growth of the DA from the baseline to ANDA optimization for the on-momentum particle is 38.95%. For the subsequent momenta, the growths are 74.06%, 109.54%, and 85.41% for 0.1%, 0.2% and 0.3% dp/p, respectively.

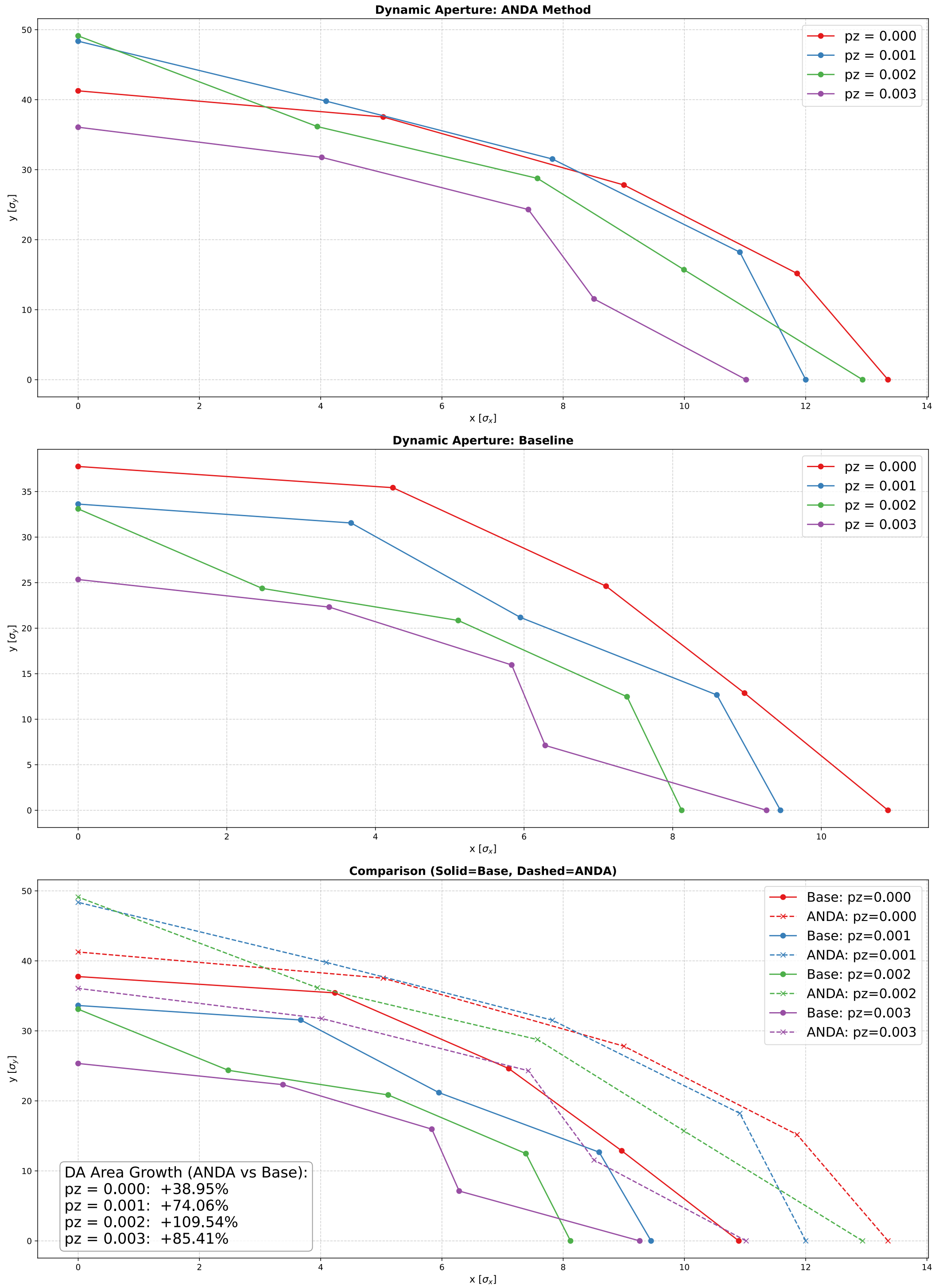

Figure 3: Top: Dynamic aperture of the post-optimization, Center: Dynamic aperture of the pre-optimization, Bottom: Comparison of the pre- and post-optimization dynamic aperture.

5 Conclusion

A method of increasing the dynamic aperture using the phase independent calculation of the the dynamic aperture to guide the optimization. The optimization utilizes the strength of the sextupoles and octupoles and the static Twiss parameters at each of the nonlinear elements to determine the local dynamic aperture. From the analytical and tracking results, it can be conclude that the horizontal dynamic aperture increased 38.95% with 4D+1 tracking.

6 Acknowledgments

I thank S. Peggs, R. Seviour, W. Fischer, Y. Luo, and D. Xu for comments and questions in reviewing this tech note.

A Diagnostic Table

Table 2: Cumulative Sum ($A^{-2}_{\mathrm{DA,sex}}$) per Sextupole

Sextupole	Baseline (m^{-2})	Post-Optimization (m^{-2})
YI6_SXD10	1.5000×10^3	1.0000×10^3
YI6_SXF11	3.5000×10^3	2.5000×10^3
YI6_SXD12	6.0000×10^3	4.5000×10^3
YI6_SXF13	9.0000×10^3	7.0000×10^3
YI6_SXD14	1.1500×10^4	9.0000×10^3
YI6_SXF15	1.4000×10^4	1.1000×10^4
YI6_SXD16	1.6500×10^4	1.3000×10^4
YI6_SXF17	1.9000×10^4	1.5000×10^4
YI6_SXD18	2.1500×10^4	1.7000×10^4
YI6_SXF19	2.4000×10^4	1.9000×10^4
YI6_SXD20	2.6500×10^4	2.1000×10^4
YI6_SXF21	2.8000×10^4	2.2000×10^4
YI7_SXD20	3.0000×10^4	2.4000×10^4
YI7_SXF19	3.2000×10^4	2.5500×10^4
YI7_SXD18	3.4000×10^4	2.7000×10^4
YI7_SXF17	3.6000×10^4	2.9000×10^4
YI7_SXD16	3.8000×10^4	3.0500×10^4
YI7_SXF15	4.0000×10^4	3.2000×10^4
YI7_SXD14	4.2500×10^4	3.4000×10^4
YI7_SXF13	4.5000×10^4	3.6000×10^4
YI7_SXD12	4.7500×10^4	3.8000×10^4
YI7_SXF11	5.0000×10^4	4.0000×10^4
YI7_SXD10	5.2000×10^4	4.2000×10^4
YI7_SXF9	5.4500×10^4	4.4000×10^4
YO8_SXD9	5.4500×10^4	4.4000×10^4
YO8_SXF10	5.4500×10^4	4.4000×10^4
YO8_SXD11	5.4500×10^4	4.4000×10^4
YO8_SXF12	5.4500×10^4	4.4000×10^4
YO8_SXD13	5.4500×10^4	4.4000×10^4

Continued on next page

Table 2 – Continued from previous page

Sextupole	Baseline (m^{-2})	Post-Optimization (m^{-2})
YO8_SXF14	5.4500×10^4	4.4000×10^4
YO8_SXD15	5.4500×10^4	4.4000×10^4
YO8_SXF16	5.4500×10^4	4.4000×10^4
YO8_SXD17	5.4500×10^4	4.4000×10^4
YO8_SXF18	5.4500×10^4	4.4000×10^4
YO8_SXD19	5.4500×10^4	4.4000×10^4
YO8_SXF20	5.4500×10^4	4.4000×10^4
YO8_SXD21	5.4500×10^4	4.4000×10^4
YO9_SXF21	5.4500×10^4	4.4000×10^4
YO9_SXD20	5.4500×10^4	4.4000×10^4
YO9_SXF19	5.4500×10^4	4.4000×10^4
YO9_SXD18	5.4500×10^4	4.4000×10^4
YO9_SXF17	5.4500×10^4	4.4000×10^4
YO9_SXD16	5.4500×10^4	4.4000×10^4
YO9_SXF15	5.4500×10^4	4.4000×10^4
YO9_SXD14	5.4500×10^4	4.4000×10^4
YO9_SXF13	5.4500×10^4	4.4000×10^4
YO9_SXD12	5.4500×10^4	4.4000×10^4
YO9_SXF11	5.4500×10^4	4.4000×10^4
YO9_SXD10	5.4500×10^4	4.4000×10^4
YI10_SXD10	6.5000×10^4	5.5000×10^4
YI10_SXF11	8.0000×10^4	6.7000×10^4
YI10_SXD12	9.0000×10^4	7.5000×10^4
YI10_SXF13	1.0500×10^5	8.8000×10^4
YI10_SXD14	1.1500×10^5	9.6000×10^4
YI10_SXF15	1.3000×10^5	1.1000×10^5
YI10_SXD16	1.3300×10^5	1.1200×10^5
YI10_SXF17	1.4000×10^5	1.1800×10^5
YI10_SXD18	1.4200×10^5	1.2000×10^5
YI10_SXF19	1.5600×10^5	1.3200×10^5
YI10_SXD20	1.5800×10^5	1.3400×10^5
YI10_SXF21	1.6800×10^5	1.4200×10^5
YI11_SXD20	1.7800×10^5	1.5000×10^5
YI11_SXF19	1.8000×10^5	1.5200×10^5
YI11_SXD18	1.8800×10^5	1.5800×10^5
YI11_SXF17	1.8900×10^5	1.5900×10^5
YI11_SXD16	2.0100×10^5	1.7000×10^5
YI11_SXF15	2.0100×10^5	1.7000×10^5
YI11_SXD14	2.0100×10^5	1.7000×10^5
YI11_SXF13	2.0100×10^5	1.7000×10^5
YI11_SXD12	2.0100×10^5	1.7000×10^5
YI11_SXF11	2.0100×10^5	1.7000×10^5
YI11_SXD10	2.0100×10^5	1.7000×10^5

Continued on next page

Table 2 – Continued from previous page

Sextupole	Baseline (m^{-2})	Post-Optimization (m^{-2})
YI11_SXF9	2.0100×10^5	1.7000×10^5
YO12_SXD9	2.0100×10^5	1.7000×10^5
YO12_SXF10	2.0100×10^5	1.7000×10^5
YO12_SXD11	2.0100×10^5	1.7000×10^5
YO12_SXF12	2.0100×10^5	1.7000×10^5
YO12_SXD13	2.0100×10^5	1.7000×10^5
YO12_SXF14	2.0100×10^5	1.7000×10^5
YO12_SXD15	2.0100×10^5	1.7000×10^5
YO12_SXF16	2.0100×10^5	1.7000×10^5
YO12_SXD17	2.0100×10^5	1.7000×10^5
YO12_SXF18	2.0100×10^5	1.7000×10^5
YO12_SXD19	2.0100×10^5	1.7000×10^5
YO12_SXF20	2.0100×10^5	1.7000×10^5
YO12_SXD21	2.0100×10^5	1.7000×10^5
YO1_SXF21	2.0100×10^5	1.7000×10^5
YO1_SXD20	2.0100×10^5	1.7000×10^5
YO1_SXF19	2.0100×10^5	1.7000×10^5
YO1_SXD18	2.0100×10^5	1.7000×10^5
YO1_SXF17	2.0100×10^5	1.7000×10^5
YO1_SXD16	2.0100×10^5	1.7000×10^5
YO1_SXF15	2.0100×10^5	1.7000×10^5
YO1_SXD14	2.0100×10^5	1.7000×10^5
YO1_SXF13	2.0100×10^5	1.7000×10^5
YO1_SXD12	2.0100×10^5	1.7000×10^5
YO1_SXF11	2.0100×10^5	1.7000×10^5
YO1_SXD10	2.0100×10^5	1.7000×10^5
YI2_SXD10	2.4500×10^5	2.0100×10^5
YI2_SXF11	2.4500×10^5	2.0100×10^5
YI2_SXD12	2.4500×10^5	2.0100×10^5
YI2_SXF13	2.4500×10^5	2.0100×10^5
YI2_SXD14	2.4500×10^5	2.0100×10^5
YI2_SXF15	2.4500×10^5	2.0100×10^5
YI2_SXD16	2.8500×10^5	2.3500×10^5
YI2_SXF17	2.8500×10^5	2.3500×10^5
YI2_SXD18	2.8500×10^5	2.3500×10^5
YI2_SXF19	2.8500×10^5	2.3500×10^5
YI2_SXD20	3.3000×10^5	2.7000×10^5
YI2_SXF21	3.3000×10^5	2.7000×10^5
YI3_SXD20	3.3000×10^5	2.7000×10^5
YI3_SXF19	3.8000×10^5	3.0000×10^5
YI3_SXD18	3.8000×10^5	3.0000×10^5
YI3_SXF17	3.8000×10^5	3.0000×10^5
YI3_SXD16	3.8000×10^5	3.0000×10^5

Continued on next page

Table 2 – Continued from previous page

Sextupole	Baseline (m^{-2})	Post-Optimization (m^{-2})
YI3_SXF15	4.2500×10^5	3.4000×10^5
YI3_SXD14	4.2500×10^5	3.4000×10^5
YI3_SXF13	4.2500×10^5	3.4000×10^5
YI3_SXD12	4.2500×10^5	3.4000×10^5
YI3_SXF11	4.6500×10^5	3.7000×10^5
YI3_SXD10	4.6500×10^5	3.7000×10^5
YI3_SXF9	4.6500×10^5	3.7000×10^5
YO4_SXD9	4.6500×10^5	3.7000×10^5
YO4_SXF10	4.6500×10^5	3.7000×10^5
YO4_SXD11	4.6500×10^5	3.7000×10^5
YO4_SXF12	4.6500×10^5	3.7000×10^5
YO4_SXD13	4.6500×10^5	3.7000×10^5
YO4_SXF14	4.6500×10^5	3.7000×10^5
YO4_SXD15	4.6500×10^5	3.7000×10^5
YO4_SXF16	4.6500×10^5	3.7000×10^5
YO4_SXD17	4.6500×10^5	3.7000×10^5
YO4_SXF18	4.6500×10^5	3.7000×10^5
YO4_SXD19	4.6500×10^5	3.7000×10^5
YO4_SXF20	4.6500×10^5	3.7000×10^5
YO4_SXD21	4.6500×10^5	3.7000×10^5
YO5_SXF21	4.6500×10^5	3.7000×10^5
YO5_SXD20	4.6500×10^5	3.7000×10^5
YO5_SXF19	4.6500×10^5	3.7000×10^5
YO5_SXD18	4.6500×10^5	3.7000×10^5
YO5_SXF17	4.6500×10^5	3.7000×10^5
YO5_SXD16	4.6500×10^5	3.7000×10^5
YO5_SXF15	4.6500×10^5	3.7000×10^5
YO5_SXD14	4.6500×10^5	3.7000×10^5
YO5_SXF13	4.6500×10^5	3.7000×10^5
YO5_SXD12	4.6500×10^5	3.7000×10^5
YO5_SXF11	4.6500×10^5	3.7000×10^5
YO5_SXD10	4.6500×10^5	3.7000×10^5

References

[1] A. W. Chao, K. H. Mess, M. Tigner, and F. Zimmermann, *Handbook of Accelerator Physics and Engineering*. WORLD SCIENTIFIC, 2nd ed., 2013.

[2] G. Guignard, "Sextupole correction and dynamic aperture: numerical and analytical tools," tech. rep., CERN, Geneva, Switzerland, 1986.

[3] D. R. Douglas, "Dynamic aperture calculations for circular accelerators and storage rings," *AIP Conference Proceedings*, vol. 153, no. 1, pp. 390–473, 1987.

[4] J. Gao, "Analytical Estimation of the Dynamic Apertures of Circular Accelerators," *Nuclear Instruments and Methods in Physics Research Section A: Accelerators, Spectrometers, Detectors and Associated Equipment*, vol. 451, pp. 545–557, 05 2000.

[5] B. W. Montague, "Basic Hamiltonian Mechanics," in *CERN Accelerator School: 5th Advanced Accelerator Physics Course*, vol. I, (Geneva), p. 1, CERN, 1995.

[6] H. Goldstein, *Classical Mechanics*. Addison-Wesley, 1980.

[7] P. J. Channell, "An illustrative example of the chirikov criterion for stochastic instability," *AIP Conference Proceedings*, vol. 46, no. 1, pp. 248–259, 1978.

[8] B. V. Chirikov, "A universal instability of many-dimensional oscillator systems," *Physics Reports*, vol. 52, no. 5, pp. 263–379, 1979.

[9] J. M. Greene, "A method for determining a stochastic transition," *Journal of Mathematical Physics*, vol. 20, no. 6, pp. 1183–1201, 1979.

[10] B. V. Chirikov and V. V. Vecheslavov, "Preservation Mechanism of a Nonlinear Resonance Separatrix amid Strong Chaos," 2000.

[11] EIC Collaboration, "Electron-Ion Collider at Brookhaven National Laboratory Conceptual Design Report," Tech. Rep. BNL-221006-2021-RPP, Brookhaven National Laboratory, Upton, NY, Feb. 2021.

[12] C. Mayes, D. Sagan, and H. Slepicka, "Pytao: the python interface to tao," in *Proc. IPAC'23*, pp. 2838–2841, JACoW Publishing, Geneva, Switzerland, 2023.

[13] J. Bengtsson, "The Sextupole Scheme for the Swiss Light Source (SLS): An Analytic Approach," Tech. Rep. 9, Paul Scherrer Institut (PSI), Villegen, Switzerland, March 1997.

[14] C.-X. Wang, "Explicit formulas for 2nd-order driving terms due to sextupoles and chromatic effects of quadrupoles.," 4 2012.

[15] D. Sagan, "Bmad: A relativistic charged particle simulation library," *Nuclear Instruments and Methods in Physics Research Section A: Accelerators, Spectrometers, Detectors and Associated Equipment*, vol. 558, no. 1, pp. 356–359, 2006. Proceedings of the 8th International Computational Accelerator Physics Conference.